NASA TECHNICAL NOTE

NASA TN D-2501

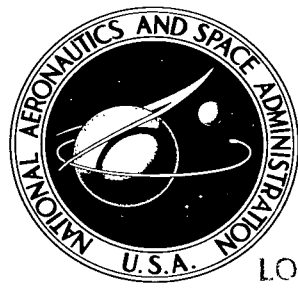

NASA TN D-2501

SURFACE PRESSURE AND TURBULENT AIRFLOW IN TRANSVERSE RECTANGULAR NOTCHES

by Jay Fox

Lewis Research Center
Cleveland, Ohio

NATIONAL AERONAUTICS AND SPACE ADMINISTRATION • WASHINGTON, D. C. • NOVEMBER 1964

SURFACE PRESSURE AND TURBULENT AIRFLOW IN TRANSVERSE RECTANGULAR NOTCHES

By Jay Fox

Lewis Research Center
Cleveland, Ohio

NATIONAL AERONAUTICS AND SPACE ADMINISTRATION

For sale by the Office of Technical Services, Department of Commerce,
Washington, D.C. 20230 -- Price $0.50

SURFACE PRESSURE AND TURBULENT AIRFLOW IN TRANSVERSE RECTANGULAR NOTCHES

by Jay Fox

Lewis Research Center

SUMMARY

Surface-pressure coefficients C_p and airflow measurements in transverse rectangular notches of length-to-height ratio $\frac{L}{H}$ from $\frac{1}{4}$ to $1\frac{3}{4}$ are presented. Free-stream speeds range from 160 to 600 feet per second. Agreement with previous low-speed measurements of C_p exists in many instances, but some unique results are also obtained. Ranges of L/H are postulated wherein similar values of C_p may be found for similar L/H. First effects of compressibility are discernible in the results. Notch flow dynamics are studied in selected notches in different L/H ranges by means of turbulence intensity measurements, mean-speed surveys, and dust patterns.

INTRODUCTION

Separated flow that is induced by a transverse rectangular cutout in the side of a body that is in a free stream can be divided roughly into three regions if the length of the cutout in the direction parallel to the stream is not too great compared with its height. The free stream, the first region, is distinguished by a low level of viscous activity (laminar or turbulent shear, or turbulent velocity fluctuations) and a high velocity. In the cutout, the second region, the velocities are less than those in the free stream, but the viscous activity can be substantial. Between these two regions there is a third region, a free-shear layer of large velocity gradients and viscous effects.

Flow dynamics in rectangular cutouts have been studied to some extent by means of wind tunnel experiments. Roshko (ref. 1) measured surface pressure in rectangular notches ($0.40 \leq L/H \leq 1.33$) in a wind-tunnel wall at low free-stream speeds (75 to 210 ft/sec). Several velocity profiles near the surfaces of the square notch seemed to indicate that a large eddy was rotating in the notch. Small corner vortices were also postulated by Roshko to complement the main vortex. Turbulent flow was present in the boundary layer ahead of the notch and in the notch.

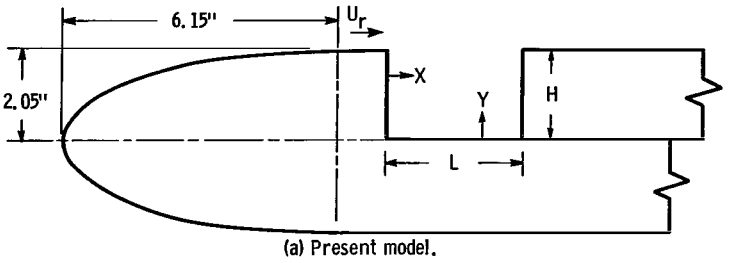

(a) Present model.

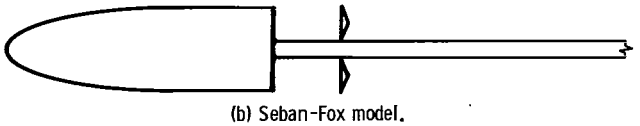

(b) Seban-Fox model.

Figure 1. - Profiles of wind tunnel models.

Charwat (ref. 2) studied the flow in long rectangular notches ($L/H > 4$) in a wind-tunnel wall. In subsonic turbulent flow, the pressure on the back end of the notch bottom increased with increasing notch length; whereas, the pressures on the front end were always near the free-stream value ahead of the notch.

Some surface pressure measurements in two notches, $L/H = 1.84$ and 3.47, were presented by Seban and Fox (ref. 3). The back sides of the notches were formed by thin fences on the wind-tunnel model shown in figure 1. Turbulent flow existed in the notch adjacent to the subsonic free stream.

The present detailed measurements of surface pressure in notches cover a greater range of geometries $\left(\frac{1}{4} \leq \frac{L}{H} \leq 1\frac{3}{4}\right)$ and free-stream speeds (160 to 600 ft/sec) than those considered by Roshko. In addition, turbulence intensity measurements, mean-speed surveys, and dust patterns at U_r equal to 160 feet per second are reported.

SYMBOLS

C_p surface-pressure coefficient, $(p - p_r)/(\rho_r U_r^2/2)$

$C_{p,t}$ total-pressure coefficient, approximately $C_p + (U_m/U_e)^2$

H notch height, in.

L notch length, in.

p static pressure

U velocity, ft/sec

U_m largest velocity located near surface of notch

U^* $U/(\tau_w/\rho)^{1/2}$

u' turbulence intensity, root-mean-square average of velocity fluctuations

X distance from front side of notch, in.

x reference length for boundary layer ahead of notch

Y distance from bottom of notch, in.

Y_1 suggested datum of Y in the free-shear layer

Y^* $Y(\tau_w/\rho)^{1/2}/\nu$

y distance normal to surface, ahead of notch, in.

δ boundary-layer thickness, in.

θ momentum thickness, $\int_0^\infty (U/U_\infty)(1 - U/U_\infty)dy$, in.

ν kinematic viscosity

ρ density

τ_w surface shear stress

Subscripts:

e edge of free stream

i incompressible flow

r measured quantity at reference location 0.25 in. ahead of notch or theoretical quantity at downstream infinity (fig. 2)

PROCEDURE

The model shown in figure 1 spanned the 6-inch width of a 6- by 9-inch wind tunnel. The model centerline coincided with the midheight of the tunnel so that the tunnel flow was divided into two streams of equal height by the elliptical nose. A 1.12-inch straight section preceded the rectangular notches, which were 2.05 inches in height H and multiples of 0.505 inch in length L. Small-diameter tubes (0.02-in. I.D.) were installed in the laminated-plastic shell of the model on the centerline between the tunnel side walls to form the pressure taps.

The stagnation chamber pressure was near atmospheric pressure, while the stagnation temperature was near 85° F. A hot-wire anemometer was used to measure mean speeds and turbulence intensities. The probe of the anemometer was calibrated in a free stream that was directed normal to the hot wire and its supporting stem (0.13-in. diam), the wire and supporting stem being perpendicular to each other. Some additional measurements of mean speeds were made with impact- and static-pressure tubes, which were always parallel to the bottom of the notch.

For correction in ordinate scale label see errata attached to front cover.

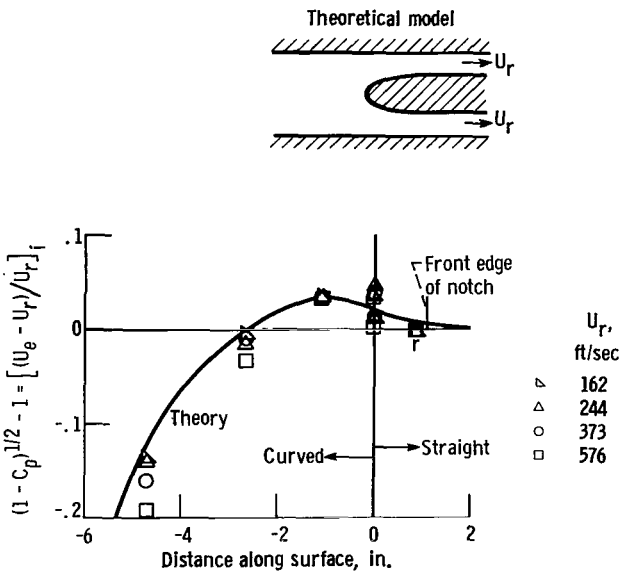

Figure 2. - Surface pressure on model nose. Curve labeled Theory is result from incompressible irrotational flow analysis applied to theoretical model shown at top. Position r is location of measured U_r.

FLOW PAST THE NOSE

Surface-pressure coefficients $C_p = (p - p_r)/(\rho_r U_r^2/2)$ are defined in relation to the free-stream conditions at the reference location, 1/4 inch ahead of the notch. A reversible, adiabatic expansion of the free stream from stagnation conditions was assumed in the calculation of ρ_r and U_r. For the experiments at U_r approximately equal to 160 feet per second, incompressible-flow relations were used to conveniently provide accurate values of U_r.

Pressure measurements on the nose surface are shown in figure 2 in the unusual form, $(1 - C_p)^{1/2} - 1$, which is equal in incompressible flow to the free-stream velocity ratio $(U_e - U_r)/U_r$. Low-speed measurements agree with the theoretical prediction that was calculated by the technique outlined in reference 4. The theory, which treats incompressible irrotational flow, was applied to the channel in figure 2. The two sets of measurements located on the boundary between the curved and straight sections were obtained from pressure taps on the upper and lower surface of the model; the difference between sets indicates the slight asymmetry of flow.

The abscissa extends in the negative direction along the curved nose of the model toward the leading edge and the stagnation point. Near the leading edge, C_p is relatively large, and it approaches the theoretical maximum value of unity for incompressible flow at the stagnation point. This corresponds to an approach of $(1 - C_p)^{1/2} - 1$ to -1. The region around the leading edge contains streamlines in the free stream that are substantially curved. The fluid particles that flow along these curved streamlines experience rapid pressure changes that become compression-expansion processes in high-speed flow. As a result, C_p departs from its low-speed value. This departure is shown in figure 2 at -4.7 and -2.6 inches as a decrease in a relatively low value of $(1 - C_p)^{1/2} - 1$, which corresponds to an increase in a high value of C_p. It is noteworthy that this high C_p is associated with a large curvature relative to the surface in a specific manner, that is, convex as viewed from the surface, and that this high C_p increases in high-speed flow. In the section Free-Stream Effects, a similar behavior of C_p in one notch is related to compressibility in the curved free stream by referring to this example on the nose.

Further remarks concerning the possibility of compressibility in a stream with a Mach number near 1/2 ($U_r \approx 558$ ft/sec) seem to be appropriate. In the present context, the term compressibility implies that the pressure variation in some local region is large enough to cause a density variation that alters

the flow field from its incompressible-flow configuration and thus alters C_p. This seems feasible when U_r is equal to 558 feet per second, since ρ_r is then 12 percent below the free-stream density at the stagnation point.

The close agreement in figure 2 between the theoretical prediction of $(1 - C_p)^{1/2} - 1$ and the low-speed measurements can be used in a deduction of the character of the free stream ahead of the notch. The theoretical flow is uniform at downstream infinity, where the velocity is U_r. The theoretical velocity along the model surface U_e approaches U_r quite rapidly after the beginning of the straight section. At reference position r, where the velocity ahead of the notch is measured, the theoretical U_e varies only 1 percent from the terminal theoretical value U_r, which corresponds to uniform flow. This implies, in view of the close agreement between the theoretical and measured values, that the actual free stream is nearly uniform across its section ahead of the notch.

The experimental velocity at the edge of the free stream U_e adjacent to the notch was measured during velocity surveys in three notches and found to be within 4 percent of U_r, as discussed in the section MEAN SPEED TRAVERSES.

UPSTREAM BOUNDARY LAYER

Ahead of the notch, the laminar nature of the boundary layer at U_r equal to 160 feet per second was ascertained by turbulence intensity measurements. The deviation between the experimental velocity profile in figure 3 and the Blasius profile for a constant value of U_e is undoubtedly a result of the wide variation of U_e on the nose, which is shown in figure 2.

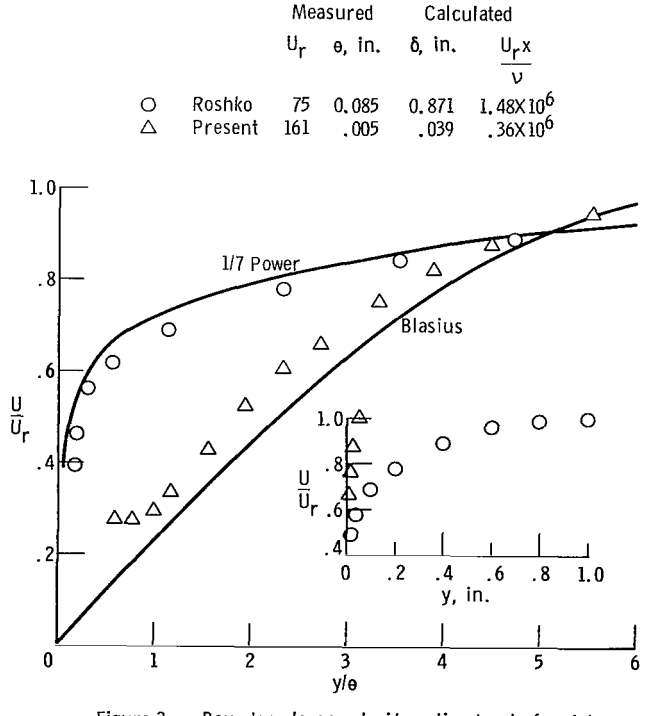

Figure 3. - Boundary-layer velocity ratio ahead of notch.

Roshko did not specifically identify the flow as being turbulent. That turbulent flow did exist in the boundary layer ahead of the 4-inch-long notch and, hence, also in the notch itself, however, is evident from the comparison between Roshko's experimental velocity profile and the 1/7-power law profile (fig. 3).

Momentum thicknesses θ for the two profiles in figure 3 are integrals of the experimental values. Formulas (ref. 5) based on the 1/7-power law profile or the Blasius profile were used to calculate boundary-layer thicknesses and

Reynolds numbers ($U_r x/\nu$) from the respective momentum thicknesses.

TRANSITION

Reference 6 showed that the transition Reynolds number in notch flow at supersonic U_e is somewhat below that for the separated flow induced by a backward facing step. Only small effects were found to result from variations in unit Reynolds number on a given model, which implies that the boundary layer ahead of the notch can be ignored in a rough approximation. In view of this, the earlier results of Chapman (ref. 7) on step models can be used to deduce an estimated transition Reynolds number of 50,000 in notches at low U_e, where the length of the notch L is taken as the characteristic length. For the lowest speed used herein ($U_e \simeq 160$ ft/sec), this estimated transition Reynolds number implies a minimum notch length of 2/5 inch for transition to turbulence. All notches in this experiment exceed that length and thus should engender turbulent flow.

TURBULENCE INTENSITY

The measurements of turbulence intensity taken at U_r approximately equal to 160 feet per second are shown in table I as u'/U_r. The value of u'/U_r in

TABLE I. - TURBULENCE INTENSITY

L/H														
1/2			1/2			1/2			3/4			1		
L, in.														
1.01			1.01			1.01			1.51			2.02		
X/L														
0.08			0.50			0.93			0.50			0.81		
X, in.														
0.08			0.50			0.94			0.75			1.64		
Y	$\frac{u'}{U}$	$\frac{u'}{U_r}$	Y	$\frac{u'}{U}$	$\frac{u'}{U_r}$	Y	$\frac{u'}{U}$	$\frac{u'}{U_r}$	Y	$\frac{u'}{U}$	$\frac{u'}{U_r}$	Y	$\frac{u'}{U}$	$\frac{u'}{U_r}$
0.003	0.19	0.009	0.005	0.50	0.019	0.003	0.10	0.004	0.003	0.23	0.029	0.003	0.23	0.036
.008	.37	.032	.400	.32	.034	.013	.53	.019	.013	.22	.054	.020	.19	.048
1.000	.25	.045	1.900	.32	.030	1.200	.44	.049	.500	.43	.059	1.100	.20	.050
1.940	.46	.037	[a]2.000	.25	.100	[a]2.000	.22	.128	1.400	.29	.031	[a]1.954	.18	.103
[a]2.045	.09	.042	2.200	.012	.012				[a]1.990	.21	.076			

[a]This location is in the middle of the free-shear layer and is the nominal location of the maximum u'/U_r.

the free stream, 0.012, is about the same as that in the laminar boundary layer ahead of the notch. In the free-shear layer of the $L/H = 1/2$ notch, a marked increase in u'/U_r above the free-stream value exists quite close to the front edge of the notch. Transition to turbulence must therefore occur within a small region adjacent to the front edge. Further evidence supporting this conclusion appears in the mean velocity profiles, which are discussed in the section FREE-SHEAR LAYER.

Turbulence measurements by other investigators in separated flow are restricted to the region behind a backward-facing step. References 8 and 9 found intensities in the middle of the free-shear layer of the same order of magnitude as those in table I, but the values of reference 10 are twice as great. On the other hand, Hsu's values just behind the step under the free-shear layer are near the present values within the notch. There may be some regularity in turbulence intensity in different separated flow configurations, but the evidence is not conclusive.

The shortest notch ($L/H = 1/4$) was not surveyed successfully; the surface measurements changed markedly when a probe was inserted. As a result, the question of whether the flow is laminar or turbulent in this notch could not be answered by turbulence intensity measurements. Surface heat-transfer measurements reported in reference 11 indicate by their variation with velocity that the flow in the $L/H = 1/4$ notch is indeed turbulent.

The results of these low-speed surveys do not, of course, establish the nature of transition and turbulence at high speed. It is noteworthy, however, that no indications of changes in transition to turbulence with speed are found in the evidence provided by the surface coefficient C_p.

SURFACE PRESSURE IN THE NOTCHES

Surface-pressure coefficients C_p are compared in this section to the results of other investigations of notches that are geometrically similar (similar L/H). Other flow parameters, such as the boundary layer ahead of the notch and the cross section of the free stream were not similar in the various experiments, but the extent to which the following comparison is successful indicates the relative unimportance of these other parameters.

For the seven notches in figure 4, C_p is displayed along the notch perimeter beginning with the front edge on the left. The front edge, the two bottom corners, and the back edge are each marked by vertical lines. The increasing length of the notches (0.505-in. increments) is shown by the increasing size of the bottom between the sides, which are fixed in height (2.05 in.). To the right of the line marking the back edge of the notch are shown C_p's that were measured on the trailing surface of the model behind the back edge of the notch.

In the shortest notch, the pressure is changed so little from the free-stream value that it suggests an analogy between this notch and a pressure tap. In fact, the "error" in the bottom of this notch is in the same direction as

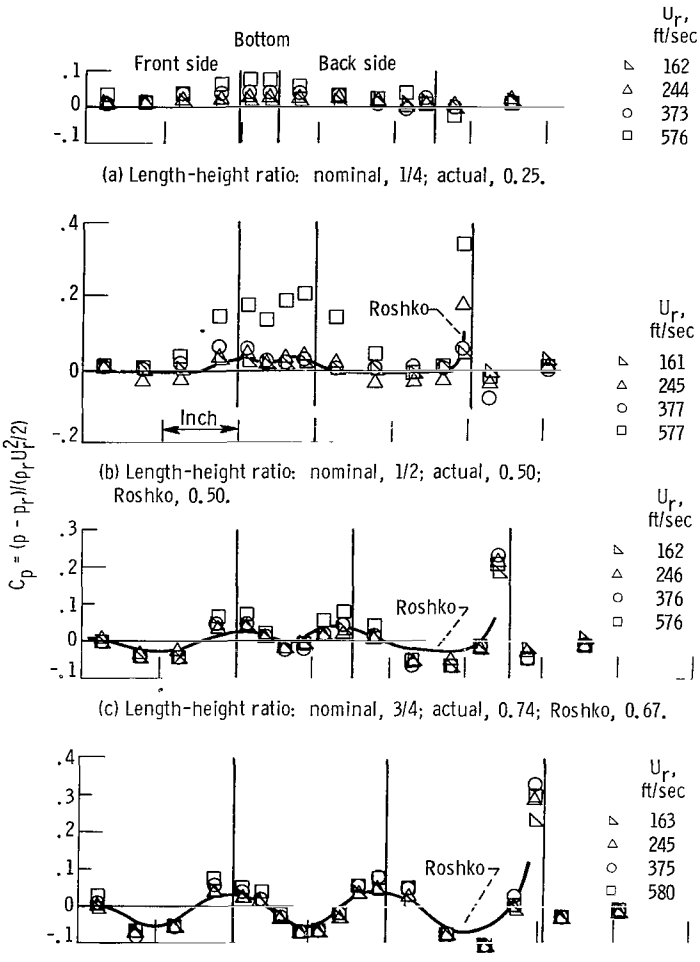

Figure 4. - Surface-pressure coefficients displayed along notch perimeter.

that measured by reference 12 in a large pressure tap, that is, in both instances the pressure is above the true free-stream pressure, which is sensed by a small pressure tap.

A high C_p at the top of the back side appears first in the $L/H = 1/2$ notch. This high C_p is associated with the impingement of some of the fluid in the free-shear layer as it returns to the notch.

Exceptional pressures in the $L/H = 1/2$ notch were recorded at the highest speed; the C_p in the bottom rose about 0.1 above the lower speed values as did the C_p at the top of the back side. During the recording of these pressures it was noted that the manometers declined during the same intervals that a distinct sound emitted from the tunnel. This suggested that a standing sound wave was raising the pressure in the bottom of the notch.

Sonic phenomena in rectangular notches (0.1 in. high) were investigated by reference 13, but surface pressures were not measured. Schlieren photographs showed sound waves emanating from the back edge of the notches, which was one of the regions in the present experiment where a sonic effect on C_p was observed. Intense sound at discrete frequencies in notches up to 1/2 inch long ($L/H = 5$) at Mach numbers greater than 2/5 was found also. The Mach number of the present experiment was 1/2 when the sonic phenomena was observed. It seems likely that the interaction of sound and pressure is similar in the two experiments; however, no other instances of sonic effects were observed in the present experiment.

Regularity of Pressure Coefficient in Ranges of Length-Height Ratio

The results of Roshko agree with the present values of C_p at most loca-

tions on the $\frac{L}{H} = \frac{1}{2}$, $\frac{3}{4}$, 1, and $1\frac{1}{4}$ notches. There is, however, a systematic deviation between the two results on the back side that is most evident in the $\frac{L}{H} = 1\frac{1}{4}$ notch.

A unique distribution of C_p appears in the $\frac{L}{H} = 1\frac{1}{2}$ notch; it is different from those in shorter and longer notches and also different from Roshko's results. Roshko noted intermittencies in C_p in the range $1.15 < L/H < 2.00$. In the present experiment, no intermittencies appeared in this L/H range.

There seem to be two ranges of L/H in which the notch flow is principally governed by L/H. Other parameters, such as the transverse extent of the free stream and the boundary layer ahead of the notch, play a secondary role in these flow regimes. Short notches ($\frac{L}{H} \leq 1\frac{1}{4}$ in the present experiment) engender one flow regime, as is evident by the comparison between Roshko's results and the present C_p in figure 4. Minor deviations between these results, such as those on the back sides, might be ascribed to the secondary parameters.

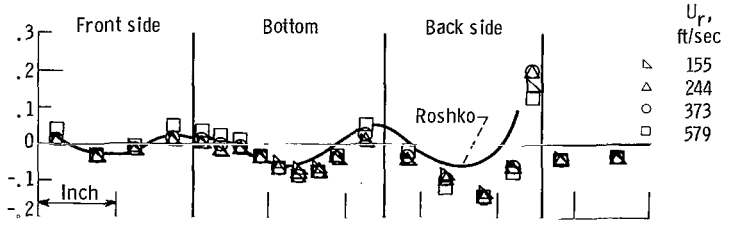

(e) Length-height ratio: nominal, $1\frac{1}{4}$; actual, 1.23; Roshko, 1.14.

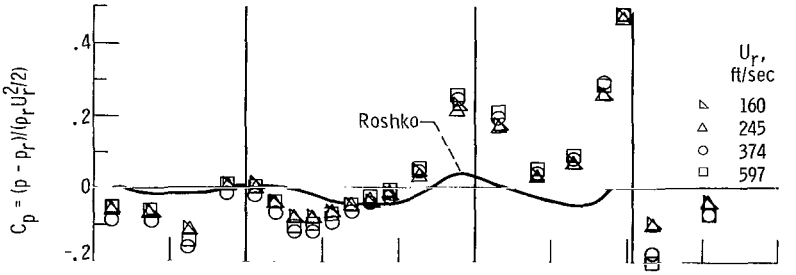

(f) Length-height ratio: nominal, $1\frac{1}{2}$; actual, 1.48; Roshko, 1.33.

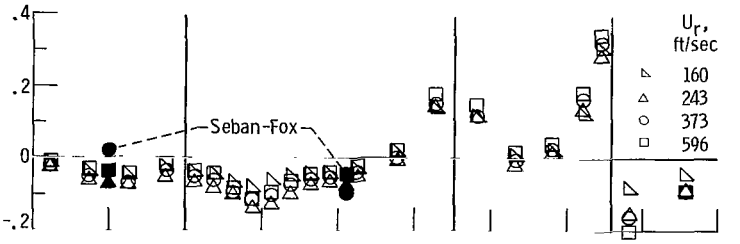

(g) Length-height ratio: nominal, $1\frac{3}{4}$; actual, 1.72; Seban-Fox, 1.84.

Figure 4. - Concluded. Surface-pressure coefficients displayed along notch perimeter.

Long notches form the other proposed range in which L/H determines the flow dynamics, as evidenced by the favorable comparison between Seban-Fox and present results in the $\frac{L}{H} = 1\frac{3}{4}$ notch. The behavior of C_p in this second range of L/H is only tentatively established since there were only two locations of measurement in the Seban-Fox experiment. There is, however, some additional evidence that tends to support the present hypothesis. Some unpublished results from the present model show that a regular variation of C_p with L/H is found in notches with $\frac{L}{H} \geq 1\frac{3}{4}$. In long notches, Roshko and Charwat also found regular variations of C_p with L/H.

Between these two ranges, the notch flow dynamics seem to be dominated by the secondary parameters. Only in this manner can the widely varying results in different experiments be rationalized. It also seems likely that the geometrical extent of this intermediate (third) regime is affected by the secondary parameters; Roshko found oscillations in notches in the range $1.15 < L/H < 2.00$, whereas, in the present experiment, unusual results were found only in the $\frac{L}{H} = 1\frac{1}{2}$ notch.

Free-Stream Effects

In the $\frac{L}{H} = 1\frac{1}{2}$ notch, the greatest deviation of the C_p distribution from the trends established by shorter and longer notches occurs on the front and back sides. These marked deviations can be used to deduce the special dynamics of the free stream adjacent to this notch. The low C_p on the front side indicates that the streamlines of the free stream are concave as viewed from the notch, that is, the free stream is curving sharply toward the notch bottom. Conversely, the high C_p on the back side shows that the streamlines in the free stream are convex to the notch or that the free stream is curving out of the notch before the back side. Behind the back edge, the low C_p indicates that a local separation bubble exists there, which causes the concave streamlines in the free stream to curve toward the surface before reattachment.

The relations between large curvature in streamlines and the pressure coefficients that were used in the foregoing discussion are the same as those found in potential theory. To rely entirely on theory to substantiate the foregoing deduction of the free-stream dynamics from the C_p on the surface of the $\frac{L}{H} = 1\frac{1}{2}$ notch is not necessary, however. Roos and Charwat (ref. 14) showed experimentally a similar curvature of the free stream in a rectangular notch in the wall of a convergent nozzle. The associated C_p's in the notch were low in the front end and remarkably high in the back end, just as the C_p's in the present $\frac{L}{H} = 1\frac{1}{2}$ notch.

Adjacent to the back edge of the $\frac{L}{H} = 1\frac{3}{4}$ notch there is also a similar curvature of the streamlines in the free stream. In this notch, the curvature can be verified indirectly by evidence from the present experiment. A comparison of C_p in the square notch, which is in the first range, with C_p in the $\frac{L}{H} = 1\frac{3}{4}$ notch, which is in the second range, is worth noting. On the back side, the C_p distribution has the same general undulation in both notches, but the pressure level is substantially higher in the $\frac{L}{H} = 1\frac{3}{4}$ notch. This implies that the free-shear layer (on the border of the free stream) dips farther into the $\frac{L}{H} = 1\frac{3}{4}$ notch and curves outward before the back edge, as do the streamlines in the adjacent free stream. A separation bubble behind the back edge is evidenced by the low C_p at that location in the $\frac{L}{H} = 1\frac{3}{4}$ notch but not in the

L/H = 1 notch. This behavior of the free-shear layer is verified in the section FREE-SHEAR LAYER by velocity surveys.

There is, therefore, an increased curvature in the streamlines of the free stream before and after the back edge of the $\frac{L}{H} = 1\frac{3}{4}$ notch. An S-shape in the streamlines near the back edge can be visualized, with curvature in one direction (out of the notch or convex as viewed from the surface) before the edge and in the other direction (toward the trailing surface or concave as viewed from the surface) after the edge. In the section FLOW PAST THE NOSE, the streamlines near the stagnation point on the nose of this model are described as curving in the same direction as those before the back edge; that is, both are convex as viewed from the surface. At the former location, the effects of compressibility were evident as an increased value of (an already high) C_p at high speeds. Since the same curvature of streamlines is present at the two locations, there can be little doubt that the increased C_p at high speeds on the back side of the $\frac{L}{H} = 1\frac{3}{4}$ notch is due to the same effect as before, namely, compressibility in the free-stream flow. After the back edge, the decreased value of the low C_p at high speed is undoubtedly also due to compressibility. In effect, this evidence of local compressibility in the free stream supports the foregoing description of the curvature in the streamlines.

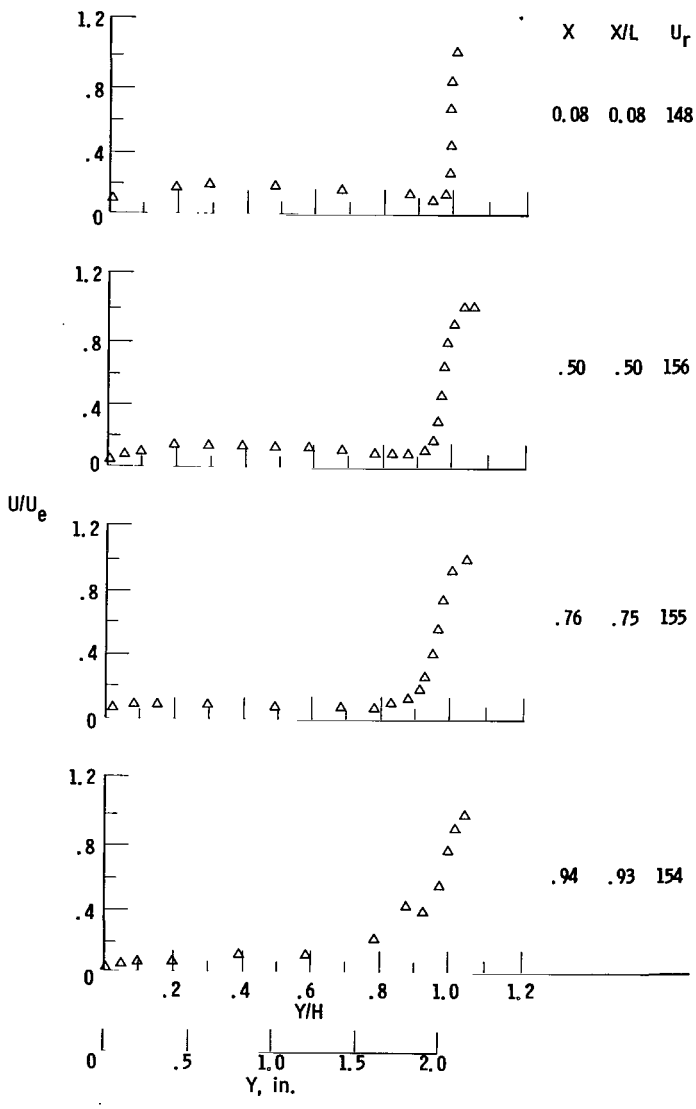

(a) Length-height ratio, 1/2.

Figure 5. - Mean speed traverses in notches. Data marked m are taken as maximum velocity ratios near bottom of notch.

MEAN SPEED TRAVERSES

The hot-wire anemometer probe that was used did not give results that were completely independent of the direction of the velocity vector.

If the stem of the hot-wire probe were absent, the orientation of the wire normal

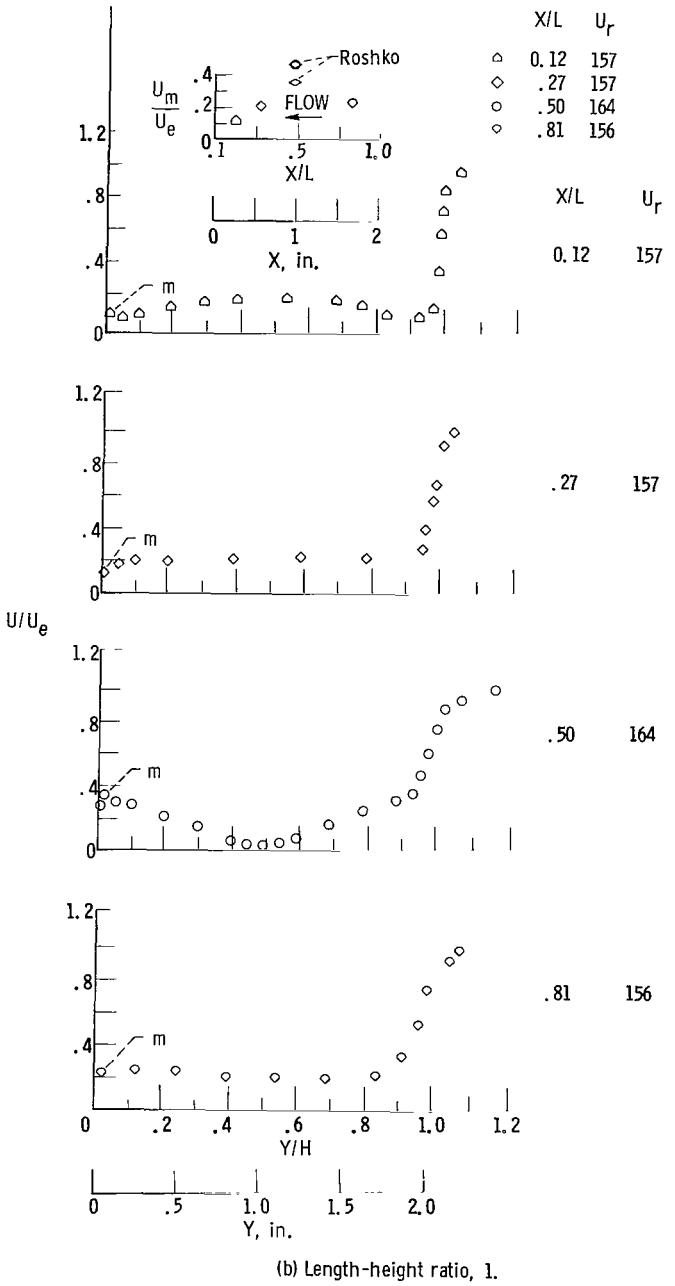

(b) Length-height ratio, 1.

Figure 5. - Continued. Mean speed traverses in notches. Data marked m are taken as maximum velocity ratios near bottom of notch.

to the profile plane of the model would have caused the wire to sense the true magnitude of the (two-dimensional) mean-velocity vector. The extent of the stem error in the results is difficult to specify, but it does seem likely that the aberration in the results in figure 5(a) (at $X/L = 0.93$, $Y/L = 0.92$) was caused by the stem. No other erratic trends are evident in the results from the $\frac{L}{H} = \frac{1}{2}$, 1, and $1\frac{3}{4}$ notches (fig. 5), and it is believed that these results give a substantially true representation of the mean speed in these notches.

The calibration of the probe was verified at the end of each traverse by a comparison of U_e with U_r; a maximum difference of 4 percent was accepted. The fact that this means of verification was feasible attests to the small variation of U_e above the notches.

SHEAR ON NOTCH BOTTOM

Velocities along the bottom of the $\frac{L}{H} = 1$ and $1\frac{3}{4}$ notches were high enough to attempt the deduction of the surface shear from their velocity profiles. The hot-wire anemometer and the impact- and static-pressure tubes were used near the bottom where both the velocity vector and the pressure tubes were parallel to the bottom surface. In addition to verifying the hot-wire results, the pressure-tube results determined the direction of the moderate-speed flow ($U/U_e > 0.15$) along the bottom to be from back to front. Hot-wire results include a correction for the heat loss to the surface by the method of reference 15.

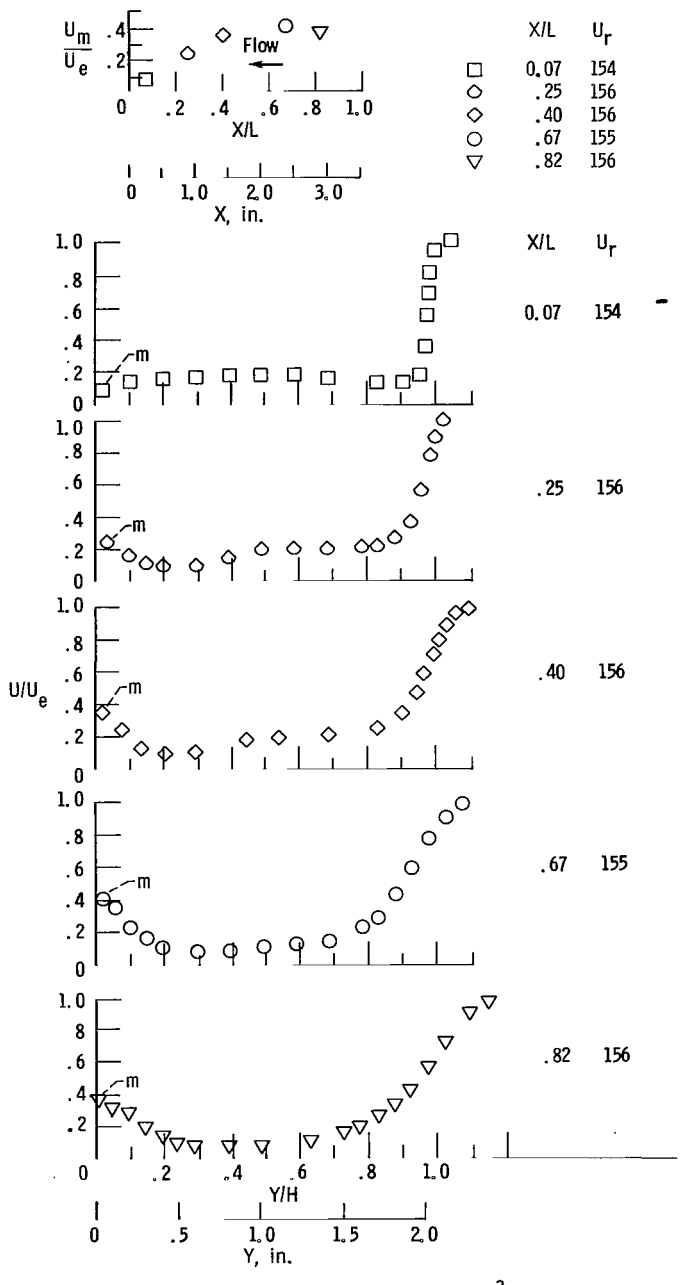

(c) Length-height ratio, $1\frac{3}{4}$.

Figure 5. - Concluded. Mean speed traverses in notches. Data marked m are taken as maximum velocity ratios near bottom of notch.

For the deduction of surface shear τ_w, the velocity profiles were compared with the Kármán profile from boundary layers, as shown in figure 6. The Kármán buffer layer profile ($U^* = -3.05 + 5 \log Y^*$, $5 \leq Y^* \leq 30$) agrees with the measurements located beyond the first data point (which is forced to match the Kármán profile) in some instances, notably at $X/L = 0.32$ in the square notch. The Blasius profile was plotted in $U^* - Y^*$ coordinates after constructing a friction coefficient $(\tau_w/\rho)^{1/2}/U_m$, where $(\tau_w/\rho)^{1/2}$ is the deduced friction velocity (from the plot) and U_m is the measured maximum velocity near the surface. Neither profile compares as well with the measured velocities in the $\frac{L}{H} = 1\frac{3}{4}$ notch as with those in the square notch. This difference in character of the measured velocity profiles may be taken as another indication of the difference in flow regimes in the two notches. Shear results by Roshko and Seban and Fox compare reasonably well with the present results, as shown in figure 6.

FREE-SHEAR LAYER

In figure 7, the lines or contours of constant velocity drawn from the traverse results (figs. 5(b) and (c)) show the behavior of the free-shear layer that was deduced from C_p distributions in the section Free-Stream Effects, namely, the free-shear layer enters farther into the $\frac{L}{H} = 1\frac{3}{4}$ notch than into the square notch and turns outward before the back edge.

The straight-line contours that are drawn between the first two traverse locations form a virtual origin for the free-shear layer by their intersection

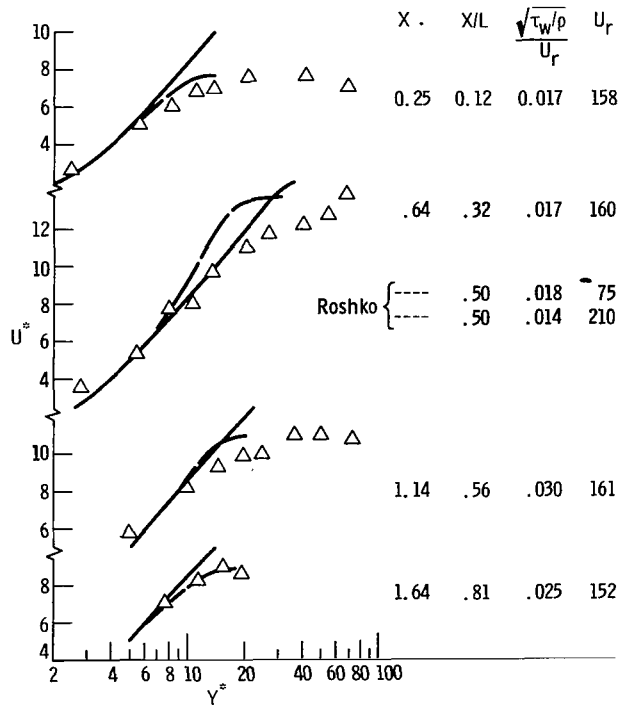

(a) Length-height ratio, 1.

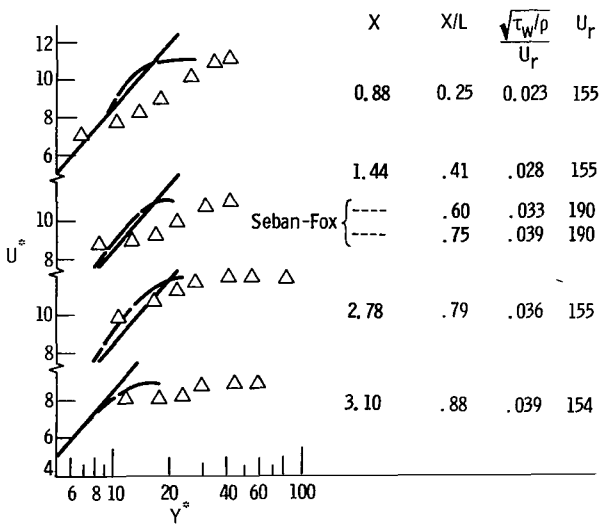

(b) Length-height ratio, $1\frac{3}{4}$.

Figure 6. - Shear on notch bottom. Solid curve is Kármán boundary layer profile. Dashed curve is Blasius laminar boundary layer profile plotted with shear listed and U_m as free-stream velocity.

near the front edge of the notches. This straight-line spreading is a well-known characteristic of turbulent free-shear layers (ref. 5). As such, it implies that the transition to turbulence in the present free-shear layer occurs quite near the front edge because of the location of the virtual origin (fig. 7).

A similarity between the first two velocity traverses on a Y/X scale is also implied by this intersection of the straight contours. These straight contours can provide a test for similarity in the back velocity traverses if they are extended to the back traverse locations, as shown in figure 7 by dashed lines. In the present view, the back velocity traverses are similar to the front traverses if the measured contours at the back traverse locations can be shifted along the line of traverse (X = constant) to coincide with the respective dashed lines. Formally, this is similarity on a $[Y - Y_1(X)]/X$ basis. This similarity can be tested by a comparison of the spacing between the measured contours with the spacing between the respective dashed lines. In the $\frac{L}{H} = 1\frac{3}{4}$ notch, similarity is maintained across the notch, but it is not maintained in the square notch. The initial spread of the contours in the square notch is greater than the spread near the back traverse locations. This difference between the contours in the $\frac{L}{H} = 1$ and $1\frac{3}{4}$ notches is interpreted as another indication of the different flow regimes in the two notches.

TOTAL-PRESSURE COEFFICIENT

Along the notch surfaces, the pressure-velocity effects, as distinguished from viscous effects, are measured by the total-pressure coefficient:

$$C_{p,t} = C_p + \left(\frac{U_m}{U_r}\right)^2 \simeq C_p + \left(\frac{U_m}{U_e}\right)^2$$

where U_m is the local maximum velocity near the surface. That $C_{p,t}$ is the parameter in Bernoulli's equation, which remains constant along a streamline in inviscid incompressible flow, should be noted. In viscous low-speed flow, $C_{p,t}$ can vary along a streamline as a result of the viscous actions of momentum diffusion (shear) and turbulent dissipation of mechanical energy; in fact, its variation can be used as a measure of viscous activity.

In the present calculation of $C_{p,t}$, the streamlines are not explicitly established. Rather, the locations of U_m, as shown in figures 5(b) and (c), are assumed to be approximately on a streamline because of their closeness to another streamline, the surface. The pressure at the location of U_m is assumed to be the same as the adjacent surface pressure. The substitution of U_m/U_e for U_m/U_r, which is necessitated by the method of data reduction, probably introduces uncertainties of the same order of magnitude (say 4 percent) as those included in the foregoing assumptions. Although $C_{p,t}$, as calculated herein, is not a precise quantity, it is useful as an indicator of viscous activity.

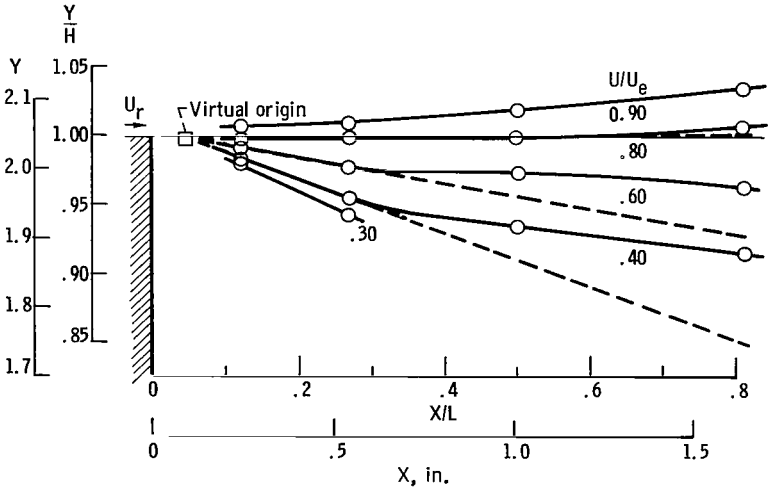

(a) Length-height ratio, 1.

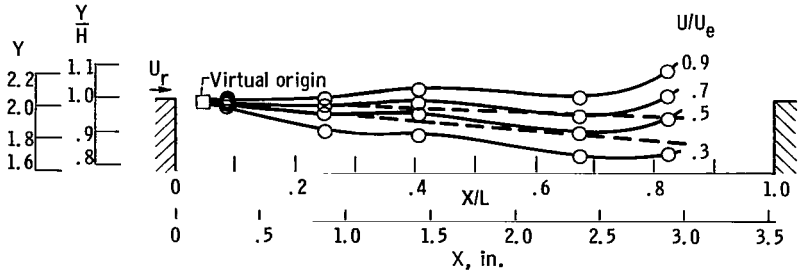

(b) Length-height ratio, $1\frac{3}{4}$.

Figure 7. - Velocity ratio contours in free-shear layer. Dashed lines are extensions of straight contours through virtual origin.

The values of $C_{p,t}$ that are calculated from C_p (fig. 4) and U_m/U_e (figs. 5(b) and (c)) are displayed along the perimeters of the $\frac{L}{H} = 1$ and $1\frac{3}{4}$ notches in figure 8. Both the square-notch results of Roshko and the present results show a gradual decline in the direction of flow, from the back side to the front side, which indicates a low level of viscous activity.

In the $\frac{L}{H} = 1\frac{3}{4}$ notch, a steeper gradient of

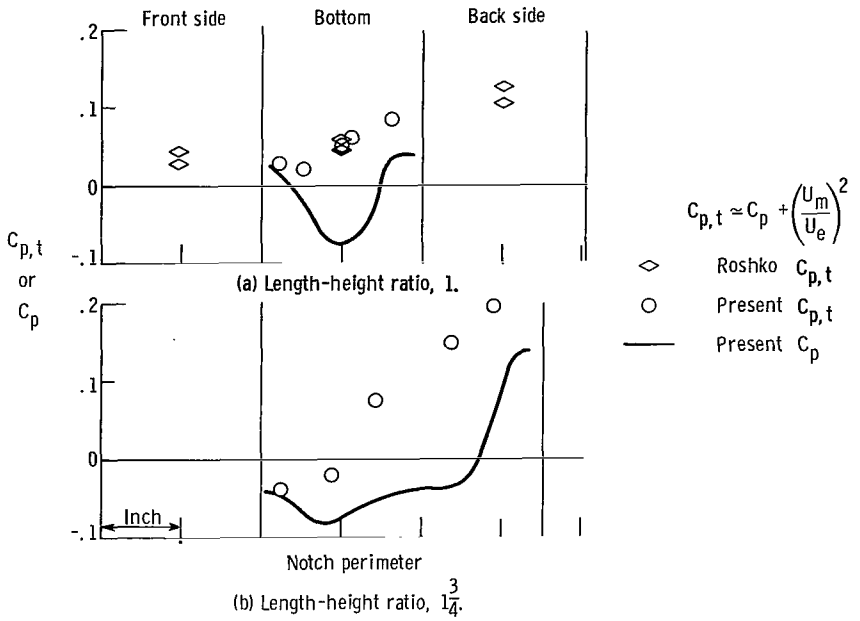

Figure 8. - Total-pressure coefficient along notch perimeter.

$C_{p,t}$ accompanies a much larger $C_{p,t}$ at the back side. These features suggest that a greater amount of energy is extracted from the free stream and dissipated by the flow in this notch than by the flow in the square notch. The idea of different flow regimes in the two notches is supported by the dissimilarity of the two distributions of $C_{p,t}$ in figure 8.

FLOW IN SQUARE NOTCH

Roshko's interpretation of square-notch flow as being dominated by a large rotating eddy was based on velocity profiles of small extent from the surfaces, which were measured at the midpoints of the three sides of a square notch. The present profile in the center of the square notch, which is shown in figure 5(b), agrees with Roshko's profile in the region of common Y/H, near the bottom. In the present result, the linear trend of U/U_e found by Roshko is shown to extend to a very low value at the midheight; it is complemented by a linear increase in U/U_e that extends to the edge of the free-shear layer.

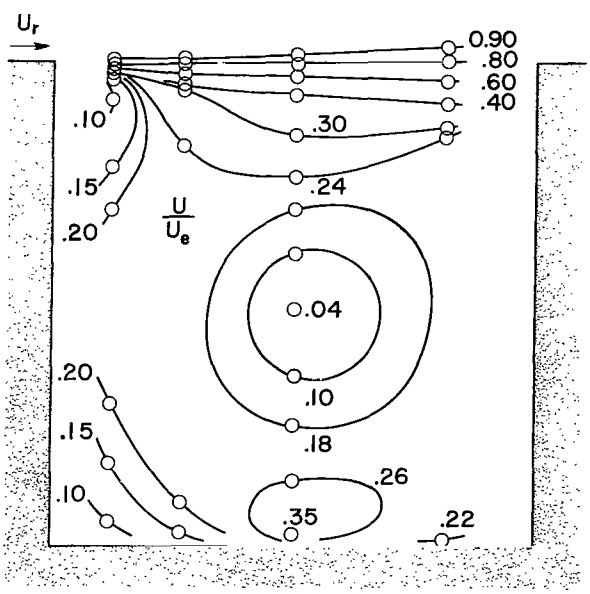

Figure 9. - Velocity ratio contours within square notch. Lines of constant velocity ratio drawn through circled measurements.

Mean speed contours, which are shown in figure 9, were constructed to examine Roshko's interpretation of square-notch flow. The small size of the region that is bounded by the circular low-speed contours around the notch center, as well as the near-zero speed at the center, suggests that the central fluid does indeed rotate. The circular high-speed contour near the bottom at midlength does not suggest a separate rotation of fluid; rather, the flow along the bottom from back to front is shown to accelerate to a peak speed at midlength and then slow near the front side.

It is interesting that evidence of a rotating eddy, such as velocities be-

ing the same on radii from some center, is found only on the central traverse. The pressure-tube measurements previously mentioned suggest that the flow continues along the bottom from back to front wherever U_m/U_e is greater than 0.15, that is, everywhere except very close to the corners. Fluid particles in the flow along the bottom, therefore, do not follow a nearly circular path in a rotation about the notch center, as a solid body; instead, the motion in the main vortex along the bottom (and probably along the sides) is parallel to the surface over much of its length, which implies that the main vortex motion is more nearly square than circular along its boundaries.

DUST DEPOSITS IN NOTCH WITH LENGTH-HEIGHT RATIO OF $1\frac{3}{4}$

The running time during traverses in the $\frac{L}{H} = 1\frac{3}{4}$ notch was long enough to clearly mark three distinct areas with dust. At the top of the back side, a heavy deposit resulted from the impingement of that portion of the free-shear layer that returned to the notch. A moderate deposit in the back corner, which extended 0.3 inch on the bottom and 0.4 inch on the back side, revealed the presence of a vortex by the abrupt thinning of the dust deposit at the edges. Lastly, a vortex was indicated in the front corner by light deposits on the front side and the bottom, which extended 0.5 inch from the corner.

The three distinct outlines were substantially two-dimensional on the central two-thirds width of the model, away from the side walls of the tunnel. Two-dimensional flow was indicated thereby, at least in the regions where the main notch flow had undergone the sharp turns that raised the surface pressure as well as produced dust deposits. The corner vortices can be considered regions of low-speed flow that bridge the gap between the separation and reattachment of the main notch flow as it rounds the turn in the corners.

CONCLUDING REMARKS

The flow studies in the $\frac{L}{H} = 1$ and $1\frac{3}{4}$ notches generally support the concept of different flow regimes in notches in the ranges $\frac{L}{H} \leq 1\frac{1}{4}$ and $\frac{L}{H} \geq 1\frac{3}{4}$. Between these ranges, C_p is not uniquely specified by L/H alone.

Roshko's evidence of a large vortex in the square notch is reproduced and extended. The new evidence implies that the large vortex motion is nearly square along its boundaries, the notch surfaces.

Lewis Research Center
National Aeronautics and Space Administration
Cleveland, Ohio, July 14, 1964

REFERENCES

1. Roshko, Anatol: Some Measurements of Flow in a Rectangular Cutout. NACA TN 3488, 1955.

2. Charwat, A. F., Roos, J. N., Dewey, F. C., and Hitz, J. A.: An Investigation of Separated Flows. Pt. 1. The Pressure Field. Jour. Aerospace Sci., vol. 28, no. 5, May 1961, pp. 457-470.

3. Seban, R. A., and Fox, J.: Heat Transfer to the Air Flow in a Surface Cavity. Proc. 1961-1962 Heat Transfer Conf., ASME, 1963, pp. 426-431.

4. Woods, L. C.: The Theory of Subsonic Plane Flow. Cambridge Univ. Press, 1961.

5. Schlichting, H.: Boundary Layer Theory. Fourth ed., McGraw-Hill Book Co., Inc., 1960.

6. Larson, Howard K., and Keating, Stephen J., Jr.: Transition Reynolds Numbers of Separated Flows at Supersonic Speeds. NASA TN D-349, 1960.

7. Chapman, Dean R., Kuehn, Donald M., and Larson, Howard K.: Investigation of Separated Flows in Supersonic and Subsonic Streams with Emphasis on the Effect of Transition. NACA Rep. 1356, 1958.

8. Abbot, D. E., and Kline, S. J.: Experimental Investigation of Subsonic Turbulent Flow Over Single and Double Backward Facing Steps. Jour. of Basic Eng. Trans. ASME, ser. D, vol. 84, Sept. 1962, pp. 317-325.

9. Tani, I.: Experimental Investigation of Flow Separation Over a Step. Boundary Layer Research, Görtler, H., ed., Springer-Verlag (Berlin), 1958, pp. 377-386.

10. Hsu, H. C.: Characteristics of Mean Flow and Turbulence at an Abrupt Two-Dimensional Expansion. Ph.D. Thesis, State Univ. of Iowa, 1950.

11. Fox, J.: Heat Transfer in Separated Flow. Ph.D. Thesis, Univ. Calif., 1963.

12. Shaw, R.: The Influence of Hole Dimensions on Static Pressure Measurements. Jour. of Fluid Mech., vol. 7, Apr. 1960, pp. 550-564.

13. Krishnamurty, K.: Acoustic Radiation from Two-Dimensional Rectangular Cutouts in Aerodynamic Surfaces. NACA TN 3487, 1955.

14. Roos, J. N., and Charwat, A. F.: The Effect of an External Pressure Gradient on a Separated Region. Jour. Aerospace Sci., vol. 29, no. 3, Mar. 1962, pp. 370-371.

15. Wills, J. A. B.: The Correction of Hot-Wire Readings for Proximity to a Solid Boundary. Jour. Fluid Mech., vol. 12, Mar. 1962, pp. 388-396.

NASA-Langley, 1964 E-2503

"The aeronautical and space activities of the United States shall be conducted so as to contribute . . . to the expansion of human knowledge of phenomena in the atmosphere and space. The Administration shall provide for the widest practicable and appropriate dissemination of information concerning its activities and the results thereof."

—NATIONAL AERONAUTICS AND SPACE ACT OF 1958

NASA SCIENTIFIC AND TECHNICAL PUBLICATIONS

TECHNICAL REPORTS: Scientific and technical information considered important, complete, and a lasting contribution to existing knowledge.

TECHNICAL NOTES: Information less broad in scope but nevertheless of importance as a contribution to existing knowledge.

TECHNICAL MEMORANDUMS: Information receiving limited distribution because of preliminary data, security classification, or other reasons.

CONTRACTOR REPORTS: Technical information generated in connection with a NASA contract or grant and released under NASA auspices.

TECHNICAL TRANSLATIONS: Information published in a foreign language considered to merit NASA distribution in English.

TECHNICAL REPRINTS: Information derived from NASA activities and initially published in the form of journal articles.

SPECIAL PUBLICATIONS: Information derived from or of value to NASA activities but not necessarily reporting the results of individual NASA-programmed scientific efforts. Publications include conference proceedings, monographs, data compilations, handbooks, sourcebooks, and special bibliographies.

Details on the availability of these publications may be obtained from:

SCIENTIFIC AND TECHNICAL INFORMATION DIVISION

NATIONAL AERONAUTICS AND SPACE ADMINISTRATION

Washington, D.C. 20546